drones

MDPI

Article

UAV-Based Pseudolite Navigation System Architecture Design and the Flight Path Optimization

Ruocheng Guo [1,2], Hong Yuan [1,*], Yang Zhang [1,*], Xiao Chen [1] and Guanbing Zhang [1,2]

[1] Aerospace Information Research Institute, Chinese Academy of Sciences, Beijing 100094, China; guoruocheng21@mails.ucas.ac.cn (R.G.); chenxiao@aircas.ac.cn (X.C.); zhangguanbing22@mails.ucas.ac.cn (G.Z.)
[2] School of Electronic, Electrical and Communication Engineering, University of Chinese Academy of Sciences, Beijing 100049, China
* Correspondence: yuanhong@aircas.ac.cn (H.Y.); zhangyang@aircas.ac.cn (Y.Z.)

Abstract: In a scenario where GNSS signal is blocked due to interference or occlusion, it is of considerable value to establish a regional navigation system providing emergency services for ground users by using long-endurance and long-range fixed-wing Unmanned Aerial Vehicles (UAVs). The main work of this paper consists of two parts. First, we designed a set of UAV-based pseudolite navigation system (UAV-PNS) architecture based on fixed-wing UAVs. Then, considering the flight cost of the UAV swarm, the optimization of the UAV swarm's flight path aimed at improving regional navigation performance was studied. In this paper, the fitness functions for UAVs' flight path optimization are proposed, taking into account the navigation and positioning performance, the aircraft utilization rate of UAVs under flight constraints, and the response speed of the system to the emergency mission. Based on this, an acceptance–rejection mutated non-dominated sorting genetic algorithm III (ARMNSGA-III) is proposed for the UAVs' flight path optimization. The research results show that the flight path strongly guarantees navigation service performance with constraints on the operating cost. The ARMNSGA-III proposed in this paper can provide a 44.01% algorithm timeliness improvement compared to the NSGA-III in the flight path optimization, supporting rapid establishment and continuous service of the UAV-PNS in emergency scenarios.

Keywords: UAV; pseudolite navigation; NSGA-III; flight path optimization

check for updates

Academic Editor: Oleg Yakimenko

Received: 13 January 2025
Revised: 7 February 2025
Accepted: 11 February 2025
Published: 12 February 2025

Citation: Guo, R.; Yuan, H.; Zhang, Y.; Chen, X.; Zhang, G. UAV-Based Pseudolite Navigation System Architecture Design and the Flight Path Optimization. *Drones* **2025**, *9*, 134. https://doi.org/10.3390/drones9020134

Copyright: © 2025 by the authors. Licensee MDPI, Basel, Switzerland. This article is an open access article distributed under the terms and conditions of the Creative Commons Attribution (CC BY) license (https://creativecommons.org/licenses/by/4.0/).

1. Introduction

With the rapid development of Global Navigation Satellite System (GNSS), navigation, positioning, and timing are increasingly integrated into human life, playing an even more important role in both the economy and military affairs [1]. However, the GNSS constellation is located in medium to high orbits; the satellites are far from the Earth's surface, resulting in low signal power at ground level. This makes GNSS signals susceptible to multipath effects, interference, and spoofing, which can lead to degraded service capability or even failure. Pseudolite navigation systems (PNS) transmit signals similar to GNSS, allowing users to receive pseudolite signals for positioning. These systems offer advantages such as high positioning accuracy and strong anti-interference capabilities [2], making PNS an effective backup in GNSS-denied environments. Currently, PNS primarily rely on ground-based PNS, which involve establishing pseudolite ground stations to broadcast navigation signals [3]. For example, the mature ground-based PNS, LOCATA, which achieves instantaneous independent positioning solutions in GNSS-denied environments

and sub-centimeter position accuracy [4,5]. The service performance of ground-based PNS is highly dependent on the density of ground station deployment. However, the construction of these systems is influenced and constrained by geographical conditions, facing challenges in mountainous and oceanic regions, leading to a weak service performance in complex environments [6], which greatly limits the applicability of ground-based PNS.

In recent years, the rapid development of Unmanned Aerial Vehicles (UAVs) has been increasingly used in navigation and communication fields [7,8]. Compared to ground-based PNS, air-based PNS utilize UAVs and other airborne carriers to broadcast navigation signals [9], which provide advantages such as strong emergency deployment capabilities, wide signal coverage range, and flexible deployment that is not restricted by ground environmental conditions [10,11]. Moreover, the network topology of UAV-based PNS is flexible and adaptable, allowing dynamic adjustments in platform configuration and distribution based on user service characteristics, enabling on-demand utilization of UAV pseudolite station resources. In contrast to ground-based PNS, the fixed-wing UAVs flying at an altitude of several kilometers allow similar navigation signal power at ground level from different UAVs, thus mitigating the effects of the near–far problem in ground-based PNS. However, there are two major technical challenges associated with air-based PNS, which greatly restrict its development. The first is the establishment and maintenance of a spatiotemporal reference for airborne platforms. This issue is typically not a concern when GNSS are available [12], but in GNSS-denied environments, it needs to be addressed through other means, which has attracted attention from scholars in the field [13,14]. This paper does not involve this issue but will discuss it in future articles. The second technical challenge comes from UAV platforms' limited range and endurance, necessitating multiple batches of UAVs to relay flights as maintaining continuous navigation service for ground users. As a result, current research on dynamic deployment and flight path optimization for air-based PNS remains limited to a small number of pseudolites self-organizing networks with low-dynamic platforms, primarily consisting of airships and rotorcraft UAVs [9,10,15,16]. It is worth noting that although rotorcraft UAVs have the capability of hovering, which can simplify the flight path optimization problem to some extent, the generally short flight duration of rotorcraft UAVs makes long-term ground navigation service relatively costly. Therefore, this paper primarily considers the flight path optimization problem of fixed-wing UAV swarms in providing navigation services to ground users.

The optimization design of a UAV swarm flight path is fundamental to establishing a regional UAV-PNS. From the perspective of users, the optimized flight path should result in minimal Dilution of Precision (DOP) factors for all potential ground users within the service region, maintaining spatial and temporal stability [17]. From the viewpoint of system construction and operation, the optimized flight path results should minimize the required swarm size and flight costs [18]. The constellation design of GNSS (both medium/high orbit and low orbit) is constrained by the fundamental laws of satellite orbital dynamics [19], and the design methods are relatively mature. In ground-based PNS, the station layout problem is essentially a static issue; rotorcraft UAVs can remain at fixed points, which also makes the use of rotorcraft UAVs as broadcasting stations similar to ground-based PNS and relatively straightforward [14,16]. In contrast, the non-hovering resident characteristics of fixed-wing UAVs makes the corresponding base station layout problem no longer a static problem. Moreover, due to the flexibility of fixed-wing UAVs, the corresponding base station layout problem can no longer be fully copied from the relevant design methods of GNSS. Therefore, the flight path optimization problem of UAV swarms in fixed-wing air-based navigation systems is fundamentally different in boundary conditions constraints from those in GNSS or ground-based PNS.

The boundary condition constraints of fixed-wing UAVs' flight path optimization requires attention. Essentially, whether it is the UAV flight path optimization problem in UAV-PNS, ground-based pseudolite layout optimization problem, or GNSS constellation design, all those multivariable optimization problems with multiple constraints fall into NP-hard problems in the field of computer science [19]. Some scholars seek optimal solutions by adjusting system parameters based on engineering experience [20–22]. As system scales continue to expand, more sophisticated random search strategies are needed to find better solutions; these methods are commonly referred to as random search algorithms, such as the genetic algorithm (GA) and its improved versions (the non-dominated sorting genetic algorithms, especially NSGA-II and NSGA-III) [19,23–25], particle swarm optimization [26], etc. In recent years, artificial intelligence methods have been widely applied to solve nonlinear time-varying problems which cannot be directly modeled; many researchers also use reinforcement learning approaches for such issues [27,28]. The evaluation of algorithms typically focuses on two aspects: whether the algorithm can find the optimal solution, and the computational resources and time required to find that solution [15]. The ability of an algorithm to find the optimal solution is equally important for fixed-wing UAV-PNS, GNSS, and ground-based PNS. However, regarding computational effort and solution time, GNSS and ground-based PNS are generally used for fixed scenarios, allowing for prolonged investment of time and computational resources to optimize station layouts in engineering practice [29]. In contrast, fixed-wing UAV-PNS are typically employed in emergency scenarios, such as natural disasters or when existing navigation systems are temporarily unavailable [30,31], requiring dynamic adjustments to a UAV swarm flight path based on changing user demands. This places great demands on computational resources and solution time for flight path optimization.

Overall, current research on air-based pseudolite navigation systems has rarely considered the specific requirements for establishing regional emergency navigation systems using a fixed-wing UAV swarm. This is because, first, there is a lack of studies on application scenarios and system design for fixed-wing UAV regional navigation systems. Second, there are insufficient targeted solutions for UAV swarm flight path optimization algorithms. To address these issues, this paper first designs a UAV-PNS architecture, ensuring the orderly operation of the system as well as the accuracy and stability of ground users' positioning performance. Next, we improved the mutation module of NSGA-III with an acceptance–rejection method, thus proposing a UAV flight path optimization algorithm ARMNSGA-III, and compared it with NSGA-III. Typical scenarios are selected for algorithm simulation and validation. The main sections are arranged as follows: Section 2 introduces the application scenarios of the UAV-PNS and the system architecture, including positioning principles, performance evaluation metrics, and UAV flight path representation methods. Section 3 formulates the problem and presents the ARMNSGA-III, including chromosome encoding, the fitness function, and a population evolution strategy that considers user weights patterns for UAV flight path azimuth and speed optimization. Section 4 validates the performance of the UAV-PNS from the perspectives of UAV flight path optimization, algorithm efficiency improvement, and evaluation of factors affecting positioning. Finally, the paper summarizes the conclusions and outlines future work prospects.

2. UAV-PNS Application Scenario and System Architecture

This section consists of two parts. First, it introduces the application scenario, refining and simplifying complex real-world situations. Then, based on the application scenario, it designs the system architecture, clarifying the system's operating mechanisms, performance evaluation metrics, modeling, and representation methods.

2.1. Application Scenario

Considering a typical scenario for deploying UAV-PNS faced by regional user groups, as illustrated in Figure 1, the main elements illustrate as follows:

- The fixed-wing UAVs take off and land from a ground airport (shown as the blue triangle in Figure 1), with the airport's location information known a priori. Considering UAV-PNS are usually used in special scenarios such as disaster relief, the airport is located outside the service region.
- Ground users are situated within the defined service region (shown as the red dot in Figure 1). Without loss of generality, this discussion is based on a rectangular shape. It is assumed that the limited height differences between different users have minimal impact on DOP values and positioning accuracy, particularly considering the high operating altitude of UAVs, thus presuming that users are on the same horizontal plane at ground level. Considering different demands of users disperse on the service region, the weights of each user in the service region are different and known a priori.
- The UAV platform transmits navigation signals to the ground using a GNSS-like signal design. The spatiotemporal reference of UAV platforms is resolved through external means, such as GNSS or ground-based beacons; this paper will not discuss these in detail. Users determine their positions using the four-satellites intersection method with pseudorange measurements.
- The endurance of the UAV is affected by its altitude and speed. UAVs tend to operate within specific altitude and speed ranges to achieve maximum hover time. This study considers UAVs flying at a constant speed and altitude, determining corresponding endurance based on their speed and altitude [32]. Additionally, the impacts of turning and takeoff/landing on endurance are incorporated as constraints in the optimization [33].
- To maintain prolonged ground navigation services, multiple batches of UAVs are required to conduct relay flights.

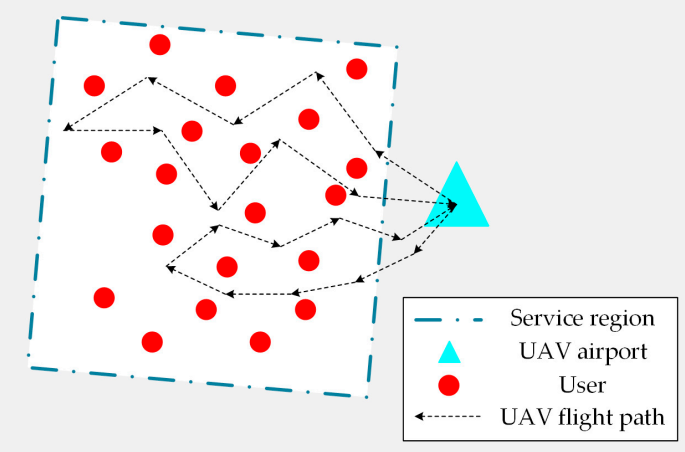


Figure 1. Typical Scenario of UAV-PNS.

UAV-PNS utilize the pseudorange measurements for distance measurement and positioning. The spatiotemporal reference for UAVs can be established using GNSS or other ground calibration methods, which will not be further discussed in this paper.

2.2. System Architecture

The following three sections will provide a detailed overview of the UAV-PNS architecture, mainly consist of three parts. First, the principles of pseudolite measurement and positioning are introduced. Next, indicators for evaluating UAV-PNS performance are further refined. Then, the characteristics of the UAV flight path will be distilled based on the application scenarios. The architecture illustrates how the system operates, providing a foundation for the design of the optimization algorithm.

2.2.1. Principle of Measurement and Positioning

The pseudolite carried by the UAV broadcasts pseudorange observations to ground users, considering the pseudorange measurement model in Single Point Positioning (SPP) [1]:

$$\rho_{si} = \|r_u - r_{si}\| + c t_u - c t_{si} + \varepsilon \tag{1}$$

ρ_{si} is the i-th pseudorange observation received by the user; each observation the user received comes from a pseudolite on a UAV. $\mathbf{r}_u = (x_u, y_u, z_u)$ and $\mathbf{r}_{si} = (x_{si}, y_{si}, z_{si})$ are the user and UAV's 3D position vectors at the observation time, respectively. t_u and t_{si} are the clock deviation between the user and the UAV to the reference time, respectively. c is the speed of light and ε is the measurement noise. It is stated that the position and clock deviation of the UAV are known to the user. Linearize (1) and write it in matrix form:

$$\Delta\boldsymbol{\rho} + \boldsymbol{\varepsilon} = \mathbf{H}\Delta\mathbf{x} \tag{2}$$

$\Delta\boldsymbol{\rho}$ is the measurement vector correction. $\Delta\mathbf{x}$ is the correction of the state vector to be estimated. $\mathbf{H}$ is the observation matrix. $\boldsymbol{\varepsilon}$ is the measurement noise vector. $\Delta\boldsymbol{\rho}$ consists of the corrections of all UAV navigation signal observations visible to the user:

$$\Delta\boldsymbol{\rho} = \begin{bmatrix} d\rho_{s1} & d\rho_{s2} & \cdots & d\rho_{sn} \end{bmatrix}^T \tag{3}$$

$\mathbf{\Delta x}$ consists of the user's 3D position corrections and the receiver's clock deviation correction multiplied by the speed of light c:

$$\Delta\mathbf{x} = \begin{bmatrix} dx_u & dy_u & dz_u & cdt_u \end{bmatrix}^T \tag{4}$$

$\mathbf{H}$ consists of the direction cosine of the unit vector from the user to the observed UAVs, presented as follows:

$$\mathbf{H} = \begin{bmatrix} \frac{x_u - x_{s1}}{\|\mathbf{r}_u - \mathbf{r}_{s1}\|} & \frac{y_u - y_{s1}}{\|\mathbf{r}_u - \mathbf{r}_{s1}\|} & \frac{z_u - z_{s1}}{\|\mathbf{r}_u - \mathbf{r}_{s1}\|} & 1 \\ \frac{x_u - x_{s2}}{\|\mathbf{r}_u - \mathbf{r}_{s2}\|} & \frac{y_u - y_{s2}}{\|\mathbf{r}_u - \mathbf{r}_{s2}\|} & \frac{z_u - z_{s2}}{\|\mathbf{r}_u - \mathbf{r}_{s2}\|} & 1 \\ \cdots & \cdots & \cdots & \cdots \\ \frac{x_u - x_{sn}}{\|\mathbf{r}_u - \mathbf{r}_{sn}\|} & \frac{y_u - y_{sn}}{\|\mathbf{r}_u - \mathbf{r}_{sn}\|} & \frac{z_u - z_{sn}}{\|\mathbf{r}_u - \mathbf{r}_{sn}\|} & 1 \end{bmatrix} \tag{5}$$

The least square is applied to solve the correction of the user's four-dimensional state vector in Formula (2):

$$\Delta\mathbf{x} = \left(\mathbf{H}^T\mathbf{H}\right)^{-1}\mathbf{H}^T\Delta\boldsymbol{\rho} \tag{6}$$

By iteratively solving the user's position and clock deviation correction, combined with the initial value of the user's state or the state value of the last epoch, the user's location can be solved.

2.2.2. System Performance Evaluation Indicators

The paper conducts the performance evaluation for the UAV-PNS from three aspects: the positioning accuracy, aircraft utilization rate, and response speed of position mission, corresponding to the instantaneous visibility and GDOP, the aircraft utilization rate of UAVs, and the establishment time of the UAV-PNS. These indicators actually represent the optimization objectives in the next section.

1. Instantaneous visibility and GDOP

The UAV-PNS pursues to provide continuous positioning service for ground users; its positioning performance can be studied from the performance of a certain time slice (epoch).

According to Formula (6) in Section 2.1, the positioning performance of the UAV-PNS is mainly determined by $\mathbf{H}$ and $\Delta\boldsymbol{\rho}$. $\Delta\boldsymbol{\rho}$ represents the ranging error of all visible UAV navigation signals; $\left(\mathbf{H}^T\mathbf{H}\right)^{-1}$ is the magnification factor from measurement error to user position error, which exactly represents the Geometric Dilution of Precision (GDOP) in UAV pseudolite positioning [1,34].

Before calculating the GDOP, the visibility judgment between the UAV and the user is first required. Figure 2 illustrates the visibility of UAV navigation signal to the ground.

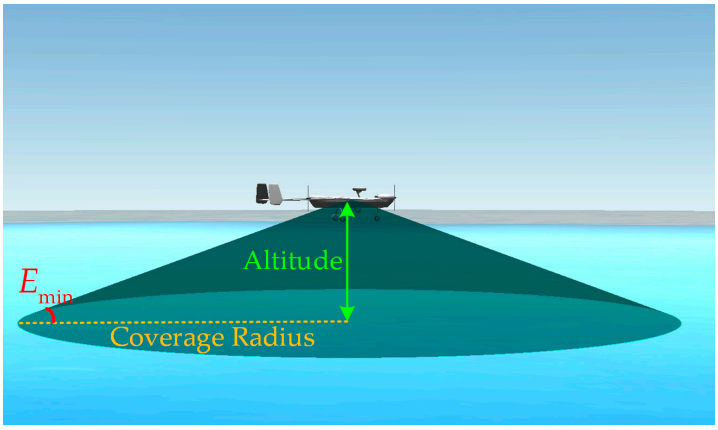


Figure 2. UAV navigation signal coverage.

The research focused on fixed-wing UAVs flying in several kilometers, so the impact of the altitude of ground users is not considered. Let the minimum observable altitude angle of the UAV be $E_{\min}$, the radius of the Earth is R_e, and the altitude of the user and the flight height of the UAV are H_u and H_s, respectively. Considering the Earth as a standard sphere, the covering hemisphere central angle from the UAV to the plane where the user is can be given by the following:

$$\theta_c = \arccos\left(\frac{R_e + H_u}{R_e + H_s}\cos E_{\min}\right) - E_{\min} \tag{7}$$

The radius of coverage of the UAV in the horizontal plane of the user's altitude is as follows:

$$R_c = (R_e + H_u)\theta_c \tag{8}$$

The relationship between the UAV's coverage radius and its altitude at different elevation mask angles is shown in Figure 3. Both the flight altitude and the elevation mask angle are positively related to the coverage radius. The paper considering the elevation mask angle as 8 degrees is common sense, while the coverage radius of the UAV is 7.1~41.7 km and its flight altitude range is 1~6 km [1,11,32].

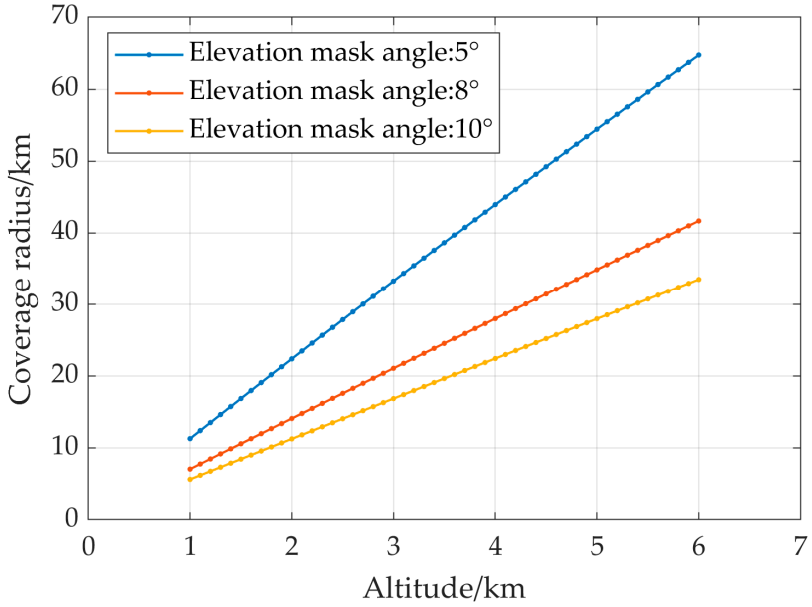


Figure 3. Relationships between UAV coverage radius and altitude.

After the visibility judgment, the GDOP is calculated based on the diagonal weight coefficient of $\left(\mathbf{H}^T\mathbf{H}\right)^{-1}$ as shown in Equations (9) and (10):

$$\mathbf{G} = diag\left(\mathbf{H}^T\mathbf{H}\right)^{-1} = diag(g_{11}, g_{22}, g_{33}, g_{44}) \tag{9}$$

$$\text{GDOP} = \sqrt{g_{11} + g_{22} + g_{33} + g_{44}} \tag{10}$$

2. The aircraft utilization rate of UAVs

An excellent UAV-PNS system design should minimize costs as much as possible, that is, the overall UAV aircraft utilization rate. Each UAV's aircraft utilization rate can be approximately formulated as the flight duration divided by endurance [35]. The factors that can affect the maximum endurance of a fixed-wing UAV include its flight speed and altitude during cruise, height changes during takeoff and landing, as well as the radius of turns, etc. [32]. This subsection considers approximate modeling of the endurance due to the main maneuvers during the UAV's flight: the speed and altitude, the turning, and the takeoff and landing.

For a UAV cruise at constant speed and altitude, its speed and altitude will approximately determine its basic endurance. According to the relationship between UAV's endurance and speed/altitude, this paper approximately models it as a quadratic function. The basic endurance is defined as E_b:

$$E_b = m_1\left(a_2 - a_1(v - v_{me})^2\right) \tag{11}$$

v is rate of flight speed, a_1 and a_2 are constants. v_{me} is the flight speed corresponding to the maximum endurance. m_1 is the scale factor.

For the endurance loss caused by UAV turns, this paper only considers constant speed and constant radius turns. It is approximated to be modeled as a function of turn time and turn radius, described as ΔE_t:

$$\Delta E_t = m_2 \frac{\theta_{TR}}{R_{TR}} \tag{12}$$

θ_{TR} is the steering angle, the R_{TR} is the turn radius. m_2 is the scale factor.

For the endurance loss from UAVs taking off and landing between the airport and specified altitude, this paper models it with altitude change during taking off and landing, as shown in ΔE_l. m_3 is the scale factor.

$$\Delta E_l = m_3 \Delta h \tag{13}$$

Above all, the endurance function due to UAV flight maneuvers is as follows:

$$E(v, h, \theta_{TR}, R_{TR}) = E_b - \Delta E_t - 2\Delta E_l \tag{14}$$

3. The establishment time of the UAV-PNS

In order to assess the response speed of the UAV-PNS to the emergency mission, the time from the beginning of the mission to system mature establishment is defined as an independent evaluation metric. Considering the characteristic of system mature establishment could be a basic positioning performance for the users, in order to satisfy the basic conditions for SPP (the user achieves quadruple coverage), it should be ensured that the number of instantaneous UAVs observed by the user reaches more than 4. Therefore, in this paper, $\overline{N_{v0}}$ is defined as the average value of the number of instantaneous UAVs observed by all the users, so the time from the mission beginning to when satisfy (15) is regarded as the establishment time of the UAV-PNS, represented as T_{SE}

$$\overline{N_{v0}} \geq 4 \tag{15}$$

2.2.3. UAV Flight Path Representation

The previous section presented the performance evaluation metrics of the UAV-PNS. According to Equations (1) and (5), the dynamic relatively positional relationship between UAV and the user significantly affects the system's navigation performance. For the modeling and representation of the flight path of the fixed-wing UAVs considered and utilized in this study, classical representations of fixed-wing UAVs' flight paths are primarily constituted by a time-varying state vector, which generally includes position, velocity, acceleration, attitude, and angular velocity [32]. However, considering the flight constraints in a fixed-wing UAV's actual flight (in the second part of Section 2.2.2), this study simplifies and models the fixed-wing UAV swarm flight path based on the fifteen-dimensional state vector information by employing a piecewise linear model, which is similar to the navigation satellite orbital models. This approach mitigates the computational burden associated with multiple time-varying parameters during flight path optimization and reduces the likelihood of converging to local optima, thereby enhancing the accuracy of navigation ephemeris. The simplified flight path parameters primarily include flight path azimuth, flight speed, and flight altitude, which will be discussed in more detail below. The flight path characteristic parameters during the fixed-wing UAV flight are illustrated in Figure 4.

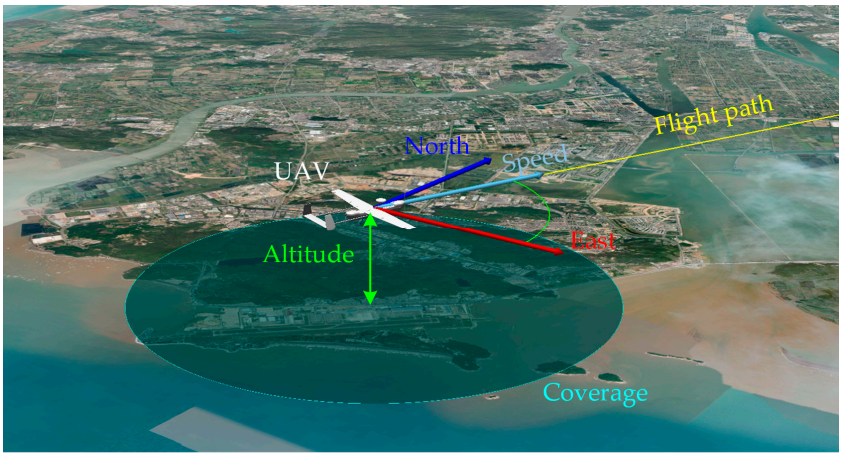


Figure 4. Fixed-wing UAV flight path characteristic parameters.

1. Flight path azimuth

The satellite orbital using inclination, right ascension of the ascending node, and argument of periapsis to determine the position of the orbital plane in ECEF, similar to satellite orbital design, in the model of the piecewise linear flight path, fixed-wing UAV's orientation, and flight range determines its service region. The angle between the UAV's orientation and the eastward direction of the geographic coordinate system is defined as the flight path azimuth. Let the number of flight paths be N^r, each path consisting of N^a line segments. The n_1-th flight path and its n_2-th segment is denoted as θ_{n_1,n_2}, and the azimuth of all flight paths form the azimuth vector $\boldsymbol{\theta}$:

$$\boldsymbol{\theta} = [\theta_{1,1}, \theta_{1,2}, \ldots, \theta_{N^r,N^a}] \tag{16}$$

2. Flight speed and flight duration

Once the UAV flight path azimuths were given, the attribution of the fixed-wing UAV flight paths should include flight speed and flight duration, which in turn determine the flight range. Flight speed and flight duration reflect the temporal evolution of the spatial relationships among of the UAV swarm. Flight speed and flight duration of all flight paths can be represented as vectors $\mathbf{V}$ and $\mathbf{T}^r$, respectively:

$$\mathbf{V} = [v_1, v_2, \ldots, v_{N^r}] \tag{17}$$

$$\mathbf{T}^r = [T_1^r, T_2^r, \ldots, T_{N^r}^r] \tag{18}$$

3. Flight Altitude

The flight altitude of the fixed-wing UAV can also be regarded as a determining attribute of the flight paths. It influences the signal coverage and the UAV's visibility. However, in this study, an increase in UAV altitude is assumed to solely enhance coverage capability. The UAV altitude is positively correlated with the service capacity of the UAV-PNS, rendering optimization of this parameter of limited significance. Therefore, this paper considers while there are differences in UAV altitudes across all flight paths to avoid collision, these differences are minimal, the optimization algorithm approximates all UAV altitudes as being uniform.

3. Optimization Algorithm for UAV Swarm Flight Path

This section focuses on the modeling and optimization methods for UAV swarm flight path optimization for the UAV-PNS. The problem modeling includes constraints and fitness function. Following the problem modeling, a search method for UAV flight paths' characteristic parameters that accounts for the prior weights of users is proposed. Based on this, a versatile improved genetic algorithm is introduced.

3.1. Problem Formulation

From the typical scenarios presented in Section 2, considering the fixed-wing UAVs require an airport for takeoff and landing, this study simplifies the problem by focusing on a single airport (the multiple airports scenario is mathematically consistent with a single-airport model; the research from the single-airport perspective does not lose generality), with all UAVs taking off from the same location. For ease of simulation, setting the simulation period T the same as the maximum endurance of UAVs as $E^{r,\max}$, the users are treated as static within this period. The study also considers batch relay organization, defining the UAV relay time interval as revisit time (RET) in reference to the concept of satellite revisit time [19]. A UAV-PNS is established to provide positioning services to users, and the fitness function constructed simultaneously reflects the various metrics discussed in Section 2.2.2, allowing for the evaluation of UAV flight path optimization results.

The constraints and fitness function will be discussed next in detail.

3.1.1. The Constraints

Based on the flight path characteristic parameters outlined in Section 2.2.3, the following assumptions are made to simplify the problem modeling:

- The total number of flight paths N^r and UAVs' flight speed and altitude are fixed, every flight path is equally divided into N^a segments, and each segment has a specific flight path azimuth, thus forming a piecewise linear path.
- The UAV will complete the entire mission from takeoff to landing in the flight duration T_n^r. For each flight path, the assigned flight speed and altitude, turnings, and altitude changes due to takeoff and landing are fixed, giving the flight path a corresponding endurance, which means the longest flight duration for UAVs. Therefore, the flight duration T_n^r should be less than the endurance, respectively.
- In order to ensure robust UAV-PNS service performance, it should maintain a stable quantity of UAVs in flight. Considering UAVs periodically take off to relay along the flight paths, each path has a fixed revisit time (RET), represented as the vector $\mathbf{T}^{RET}$ as follows:

$$\mathbf{T}^{RET} = \left[T_1^{RET}, T_2^{RET}, \ldots, T_{N^r}^{RET}\right] \tag{19}$$

Based on the aforementioned assumptions, the number of UAVs N_n^{rs} that are continuously online for the n-th flight path and the total number of UAVs N^{UAV} are calculated as follows:

$$N_n^{rs} = T_n^r / T_n^{RET} \tag{20}$$

$$N^{UAV} = \sum_{n=1}^{N^r} N_n^{rs} \tag{21}$$

Additionally, considering the UAV's flight speed range $V_{\min}^{fi}$~$V_{\max}^{fi}$ and altitude range $H_{\min}^{fi}$~$H_{\max}^{fi}$, let the airport coordinates be $(x_{airport}, y_{airport}, z_{airport})$ and the UAV's constant altitude set as h_0. Based on the UAV endurance model established in Section 2.2.2, the flight duration T_n^r for the n-th flight path is given by the following:

$$T_n^r \le E(v_n, h_0, \theta_{n,i}, R_{tr\min}) = m_1\left(a_2 - a_1(v_n - v_{me})^2\right) - m_2\frac{1}{R_{tr\min}}\sum_{i=1}^{N^a}\theta_{n,i} - 2m_3h_0 \quad (22)$$

$R_{tr\min}$ is the turning radius at the junctions of segments in the piecewise linear flight path. The condition for achieving the theoretical maximum value $T^{r,\max}$ is that the UAV flies at its maximum endurance speed v_{me}, and the entire flight only involves a straight path with a 180-degree turn, thereby minimizing the maneuvering endurance loss. Under these, the maximum endurance is expressed as follows:

$$E^{r,\max} = m_1a_2 - m_2\frac{\pi}{R_{tr\min}} - 2m_3h_0 \quad (23)$$

By organizing the above constraints, we obtain the following:

$$s.t.\ \forall n \in \{1, 2, \ldots, N^r\},\ \begin{cases} \mathbf{r}_{si}(t) = (x_{airport}, y_{airport}, z_{airport}), t = 0, T_n^r, 2T_n^r, \ldots \\ V_{\min}^{fi} \le v_n \le V_{\max}^{fi}, H_{\min}^{fi} \le h_n = h_0 \le H_{\max}^{fi} \\ T_n^r = N_n^{rs}T_n^{RET} \le E^{r,\max}, \sum_{n=1}^{N^r} N_n^{rs} \le N^{UAV} \end{cases} \quad (24)$$

3.1.2. The Fitness Function

When formulating the fitness function utilized in the algorithm, primary objectives must be thoroughly considered. According to Section 2.2.2, the objectives are the instantaneous visibility and GDOP, the utilization rate of UAVs, and the establishment time of the UAV-PNS. Then, the fitness functions can be formulated as follows, corresponding to the objectives:

1. The first fitness function reflects the continuous positioning accuracy level of the weighted users, as well as the stability of the positioning accuracy.

For the evaluation of continuous positioning performance, both the average and variability of users' continuous GDOP should be considered; the continuous GDOP could be seen as the extension of instantaneous GDOP in time. This study references commonly used fitness functions in navigation constellation design [15,19], while accumulating the weighted average and weighted standard deviation of GDOP for users within the service region, statistics of the simulation period T, including e_n epochs. Accordingly, the first fitness function F_1 is expressed as follows:

$$E_e = \frac{\sum_{i=1,j=1}^{i_{\max},j_{\max}} \rho(x_{ui}, y_{uj})\mathrm{GDOP}(x_{ui}, y_{uj}, e)}{\sum_{i=1,j=1}^{i_{\max},j_{\max}} \rho(x_{ui}, y_{uj})} \quad (25)$$

$$S_e = \sqrt{\frac{\sum_{i=1,j=1}^{i_{\max},j_{\max}} \rho(x_{ui}, y_{uj})\left[\mathrm{GDOP}(x_{ui}, y_{uj}, e) - E_e\right]^2}{\sum_{i=1,j=1}^{i_{\max},j_{\max}} \rho(x_{ui}, y_{uj})}} \quad (26)$$

$$F_1 = \sum_{e=1}^{e_n} [E_e + S_e]/e_n \tag{27}$$

The E_e and S_e represent the weighted average and weighted standard deviation of GDOP for users within the region at the e-th epoch. $\rho(x_{ui}, y_{uj})$ represents the weight of ground user in grid position (x_{ui}, y_{uj}), and GDOP(x_{ui}, y_{uj}, e) is its instantaneous GDOP at the e-th epoch.

Furthermore, if a particular grid point cannot achieve quadruple coverage, meaning that positioning computation for that epoch cannot be realized, the GDOP is set to 50 as a penalty [34]. For users with computed GDOP results greater than 50, their positioning results are considered unavailable; their GDOP is therefore set to 50.

2. The second fitness function reflects the costs of the UAV-PNS in terms of the UAVs' utilization rate.

According to Section 2.2.2, a single UAV's aircraft utilization rate can be approximately formulated as the flight duration T_n^r divided by endurance $E(v_n, h_0, \theta_{n,i}, R_{tr\min})$; in statistics for all the UAVs of the simulation period T, the second fitness function F_2 is expressed as (27); it can be seen as the average numbers of UAVs in flight

$$F_2 = \sum_{n=1}^{N^r} \frac{T_n^r}{E(v_n, h_0, \theta_{n,i}, R_{tr\min}) T_n^{RET}} = \sum_{n=1}^{N^r} \frac{N_n^{rs}}{E(v_n, h_0, \theta_{n,i}, R_{tr\min})} \tag{28}$$

3. The third fitness function reflects response speed of the UAV-PNS to the emergency mission in terms of the establishment time.

According to Section 2.2.2, the epochs from the mission beginning to the time satisfying $\overline{N_{v0}} \geq 4$ are regarded as the establishment time of the UAV-PNS, represented as T_{SE}. The third fitness function F_3 is expressed as follows:

$$F_3 = T_{SE} \tag{29}$$

Regarding the priority of the three fitness functions in the optimization algorithm, for the UAV-PNS it is essential to ensure that users meet the basic positioning accuracy F_1^b required for the task. Therefore, F_1 has the highest priority. During the optimization, after ensuring that $F_1 \leq F_1^b$, F_2, and F_3 have the same highest priority, by applying the objective normalization method from NSGA-III [36], the normalized results of F_2 and F_3 are summed to obtain the sorting and population evolution.

3.2. Principle of the Algorithm

Based on the aforementioned fitness function and constraints, this section presents the principles of the ARMNSGA-III for UAV-PNS flight path optimization. The section includes the overall algorithm framework, decision variables, and chromosome encoding, and a search strategy for decision variables.

3.2.1. Algorithm Framework

The NSGA-III could be the most famous algorithm in the GA family, fairly used in multi-objectives optimization problems [23,36,37]. This paper builds a new method, ARMNSGA-III, upon NSGA-III by presenting an improved mutation module. It effectively extracts prior information about users' weights and distribution, and models them as a specific search model, subsequently employing an acceptance–rejection sampling method to obtain mutation results, replacing the random mutation strategy in NSGA. During the population evolution, the interactions among decision variables and their impact on evaluation results are thoroughly considered. In this paper, the UAV navigation rules are

utilized to seek the optimal resolution, refining search strategies for decision variables, thereby reducing the dimensionality of the search space. By modeling the navigation rules as a specific probability density function (p.d.f), the acceptance–rejection sampling, which can be applied to generate samples as nonrandom search results reference to the given p.d.f. This approach enhances the search probability for optimal solutions while ensuring the completeness of the solutions, thereby improving algorithm efficiency. The algorithm flow is illustrated in Figure 5.

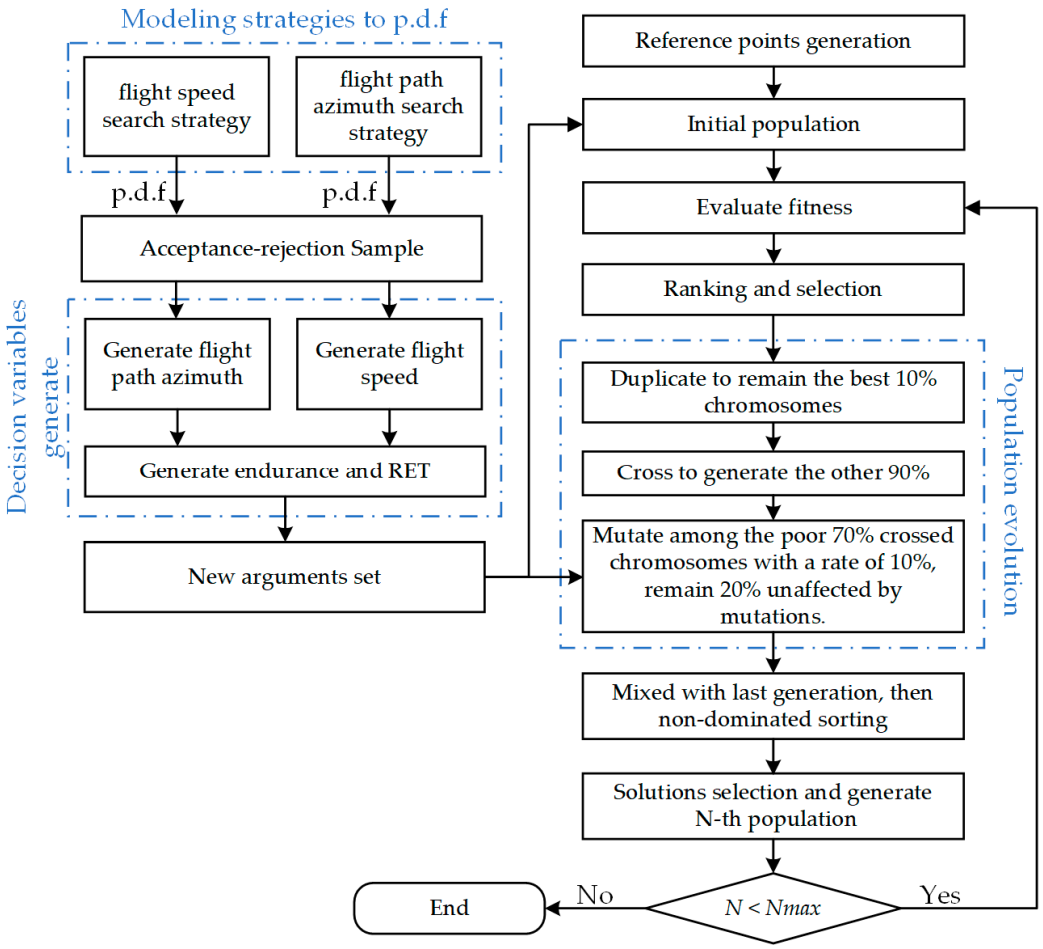


Figure 5. Framework of ARMNSGA-III.

The algorithm flow is divided into the following steps:

- Modeling potential navigation rules in the UAV-PNS as search strategies of decision variables, include flight speed and azimuth search strategy.
- Using the acceptance–rejection method to sample nonrandom search results to generate the initial population.
- Generate the reference points with three objectives: evaluate the fitness function values for the population, assign each chromosome with a rank, and select the front chromosomes for evolution.
- Cross: 10% of elite individuals are retained, while the remaining 90% undergo recombination. Mutation: 70% of the individuals with poor fitness values are mutated, utilizing the acceptance–rejection method to generate genes.
- Mix the current generation with the last generation, adopting non-dominated sorting with the reference points, keep chromosomes which are close to the reference points [38].

- The algorithm checks whether the specified number of iterations has been reached; if not, the next iteration is performed; otherwise, the algorithm concludes and exits.

3.2.2. Decision Variables and Chromosome Encoding

Each solution of the optimization problem is a chromosome within the population, which encompasses a complete set of optimization decision variables; each decision variable terms a gene. In this study, the following genes are concatenated to form a chromosome, including flight path azimuth, UAV flight speed, UAV flight duration, and RET.

$$\begin{cases} \boldsymbol{\theta} = [\theta_{1,1}, \theta_{1,2}, \ldots, \theta_{N^r,N^a}] \\ \mathbf{V} = [v_1, v_2, \ldots, v_{N^r}] \\ \mathbf{T}^r = [T_1^r, T_2^r, \ldots, T_{N^r}^r] \\ \mathbf{T}^{RET} = [T_1^{RET}, T_2^{RET}, \ldots, T_{N^r}^{RET}] \end{cases} \tag{30}$$

The chromosomes utilize floating-point encoding. Considering practical conditions, the search step size for flight speed is set to 0.1 km/h, while the search step sizes for flight duration and RET are set to 0.01 h. Under the predetermined number of UAV flight path N^r, the variables in Equation (29) constitute a complete spatial position evolution model for the UAV-PNS.

3.2.3. Search Strategy for the Decision Variables

GAs facilitate chromosome variation through operations such as cross and mutation, thereby promoting the emergence of potentially superior individuals. Cross involves the arrangement and combination of variables across different dimensions, while mutation introduces genes that may not currently exist in the genome. NSGAs primarily employ a uniform random search strategy, resulting in a limited effective space across different search dimensions in the solution space. This study focuses on flight path optimization for dozens of UAV platforms; the decision variables and objectives can be numerous and coupling, characterized by a large search dimension. To identify the effective search interval for each dimension and ultimately achieve optimal solutions, an effective search strategy is required.

To improve search efficiency, this study proposes a nonrandom search method based on the acceptance–rejection sampling method. It employs the Monte Carlo principle to generate random numbers that satisfy any probability density function (p.d.f), with the fundamental principle of conditional probability [39]. This approach provides a means to generate mutation values according to prior parameter distributions [40,41], thereby enhancing the mutation strategy. Acceptance–rejection sampling is widely used for generating samples that conform to specified probability distributions, offering a simple and rapid solution that ensures increased algorithmic search efficiency at a small computational cost. In the design of the search strategy, prior knowledge about users' weights and distribution is utilized as guidance in modeling the search strategy for the parameter, including flight path azimuth and flight speed. The p.d.f defined over the parameter search domain corresponds to the probability, thus serving for the acceptance–rejection method and outputting the decision variables mutation values. The principle is illustrated in Figure 6.

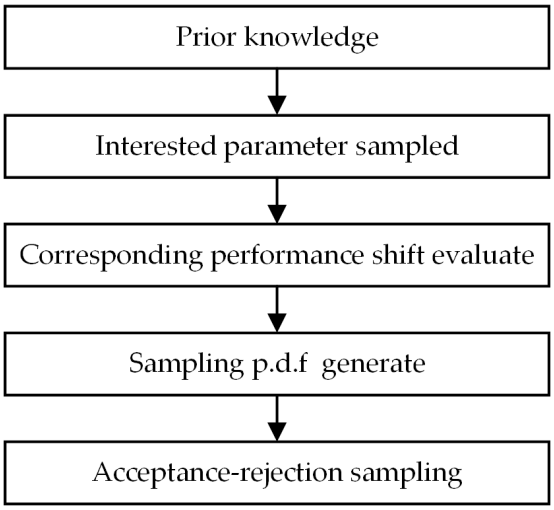


Figure 6. Principle of the searching strategy modeling.

The search strategy possesses two advantages: first, it integrates statistical characteristic analysis aligned with navigation rules to enhance search efficiency; second, the non-random sampling does not exclude non-priority solution spaces, retaining potential genes within the combined solutions, thus maintaining the completeness of the search space.

The following two parts will model the flight path azimuth and flight speed based on the principles illustrated in Figure 6.

1. Acceptance–rejection p.d.f for flight path azimuth

Intuitively, the weights and distribution of ground users are significant factors in determining the UAV flight path azimuth. Specifically, when the UAV departs from each junction of the piecewise linear flight path, it should orient toward a position prioritizing higher users' weights for pursuing potential visibility and GDOP. Consequently, an appropriate UAV flight path azimuth can be identified based on the prior weights of users within the service region. By accumulating the users' weights along the coordinate axes, the values indicate the expectation after orthogonal decomposition of the flight path azimuth.

For a specific users' weights and distribution map, under the WGS84 coordinate system, the cumulative projection of users' weights along the northward direction is ultimately projected onto the eastward coordinate axis to obtain pdf_x. Similarly, the cumulative projection along the eastward direction onto the northward coordinate axis yields pdf_y. The acceptance–rejection method is then employed to derive x_p and y_p, representing the projections of the flight path azimuth in the eastward and northward directions, respectively, thereby determining the flight path azimuth as a mutation result:

$$\theta = \arctan\frac{y_p}{x_p} \tag{31}$$

2. Acceptance–rejection p.d.f for flight speed

Users' weights and distribution are often uneven, characterized by varying distances from the UAV airport. Once the flight path azimuth is determined, the distribution of users' weights along this azimuth is known. By means of testing different flight speeds and statistically assessing the coverage users' weights, the relationship between assessed results and corresponding flight speed can serve as a p.d.f for acceptance–rejection. To discretize the velocity interval, conduct equal interval sampling within the range of flight speed:

$$V_{\min}^{fi}, V_{\min}^{fi} + v^s, \ldots, V_{\max}^{fi} \tag{32}$$

v_s is the sampling interval. Each sampled speed is used to generate a flight path segment along the azimuth. The total user coverage weights $\sum\rho$ are calculated. The coverage weights of users correspond to speed in (29):

$$\sum\rho\left(V_{\min}^{fi}\right),\sum\rho\left(V_{\min}^{fi}+v^{s}\right),\ldots,\sum\rho\left(V_{\max}^{fi}\right) \tag{33}$$

The coverage weights are used to construct an acceptance–rejection p.d.f input, characterizing the coverage and positioning capabilities corresponding to the respective flight speed. This enables an uneven search strategy during the flight speed parameter search. The flight speed acceptance–rejection sampling p.d.f is illustrated in Figure 7.

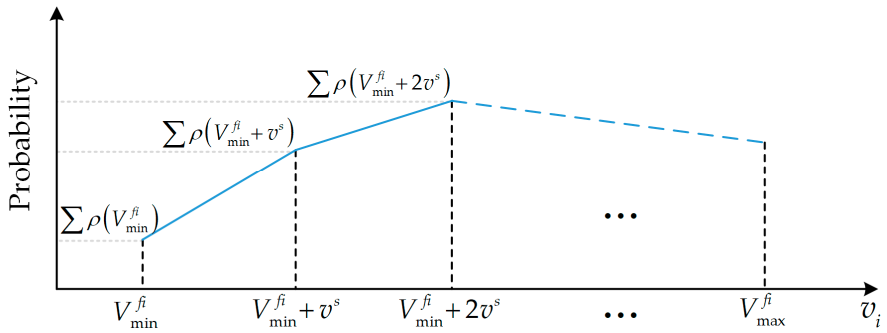


Figure 7. UAV flight speed acceptance–rejection sampling p.d.f.

Thus, the p.d.f representing the weights and distribution characteristics of users can be derived. The proposed method achieved efficient utilization of UAV resources according to users demands. For multiple airports in practical engineering, the decision variable mutation search p.d.f can be modeled for each airport, and the fitness function can be evaluated by aggregating the UAV swarm paths for all airports.

4. Simulation Design and Result Analysis

This section begins with the simulation design of the UAV-PNS, delineating the specific service region and configuring system parameters. Subsequently, UAV flight path optimization based on the ARMNSGA-III is conducted, followed by static and dynamic analyses of the algorithm's results. The performance enhancement of the ARMNSGA-III algorithm is compared to the NSGA-III.

4.1. Simulation Design

The simulation was conducted to verify the effectiveness of UAV swarm flight path optimization based on the ARMNSGA-III, then further research the impact of flight path characteristic parameters on the performance of the UAV-PNS. The content next includes the delineating of service region, the configuration of users' weights distributions, and the setting of algorithm parameters.

The simulation uses real population density distribution of a specific region as users' weights distribution [42], regarding population density in the grid as its weights. The blue dashed box presents the service region, with the coordinates of the four vertices defined as (23.0543 °N, 114.6229 °E), (23.0080 °N, 114.6692 °E), (23.1469 °N, 114.7155 °E), and (23.1006 °N, 114.7618 °E), with the airport located at (23.0250 °N, 114.7170 °E). The simulation period is set as 1 h; the unit grid size for calculating the fitness function is chosen to be 5 km. The users' weights distribution within the region is illustrated in Figure 8.

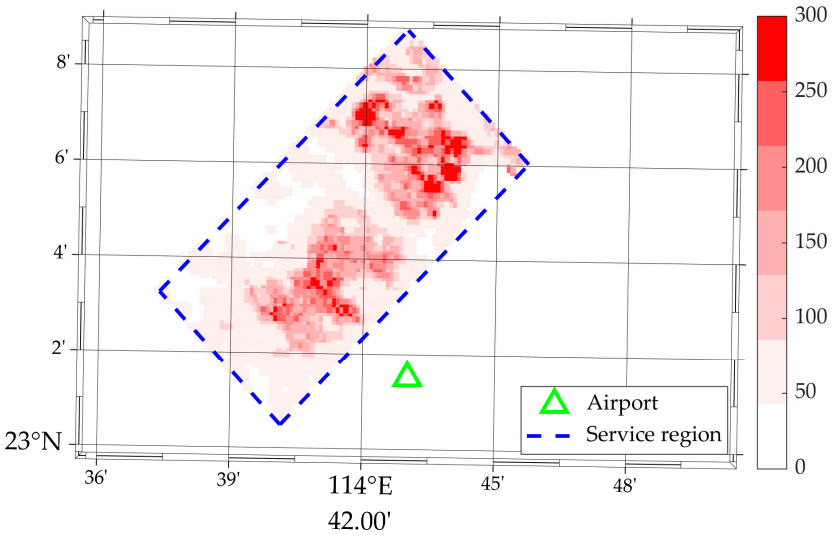


Figure 8. Users' weights for simulation. The intensity of red indicates user weights and a darker color represents higher weights. The schematic representation of users' weights.

The predetermined simulation parameter settings include a simulation period for 1 h, divided into 100 epochs. The UAV flight paths amount is fixed as eight; each flight path equally divides into 10 segments. The maximum number of available UAVs is 32. Referencing the flight speed and altitude range of medium-sized fixed-wing UAVs, the UAV speeds and altitudes ranges are set as 60 to 160 km/h and 1 to 6 km, respectively. To ensure UAV coverage, the altitude is fixed at 4 km, correspond to a 26.8 km coverage radius. The basic F_1 required by the task F_1^b is set as 20. All algorithm preset parameters are detailed in Table 1 and Figure 5. Once the flight path's characteristics are established, the relationships between endurance, range, and flight speed of the UAVs are illustrated in Figure 9, respectively.

Table 1. Simulation parameter settings.

Simulation Parameter	Value
Max number of UAVs (N^{UAV})	32
Number of flight paths (N^{UAV})	8
Piecewise linear segments (N^a)	10
Maximum flight duration of UAVs ($E^{r,\max}$)	1 h
Simulation period (T)	1 h
UAV flight speed ($V_{\min}^{fi}$~$V_{\max}^{fi}$)	60~160 km/h
UAV altitude (h_0)	4 km
Basic F_1 required by the task (F_1^b)	20
Scale factor (m_1, m_2, m_3)	1, 8.5, 0.01
Constants (a_1, a_2)	10^{-5}, 1.25
Unit grid size	5 km
GA chromosome number	100
GA iteration times	300
GA mutation probability	10%

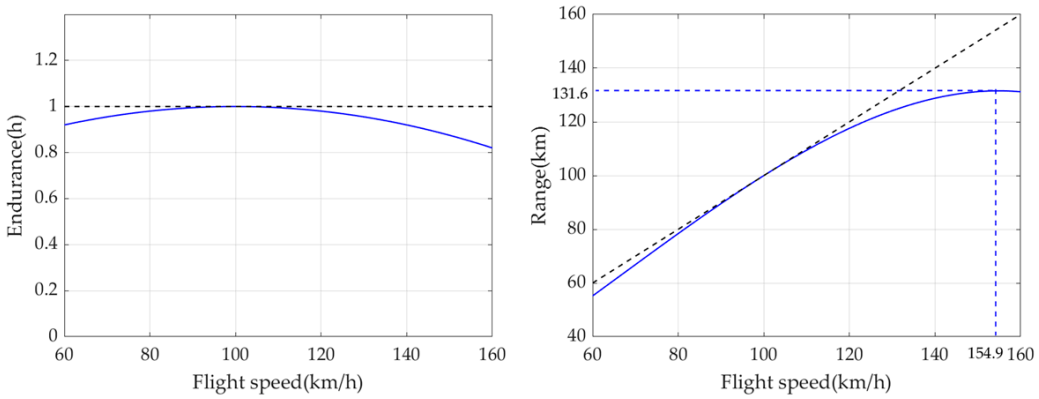


Figure 9. The relationships between endurance/range and flight speed. The longest range is 131.6 km, corresponding to the longest endurance speed v_{me} of 154.9 km/h. The black dashed line is the upbound.

4.2. Results Analysis and Evaluation

4.2.1. Presentation of Simulation Results

Figure 10 presents the simulation results of UAV flight path optimization. After numerous iterations, the results can be considered approximately optimal. Figure 10a shows the variation of fitness functions during the algorithm iterations (as the prior stated in Section 3.1.2, fitness function 1 has the highest prior before reach the basic position accuracy F_1^b). Figure 10b displays the top-performing individuals (the top 1% based on the normalized ASF equation of NSGA-III [36]) from the output population of the algorithm; it reveals the potential Pareto front.

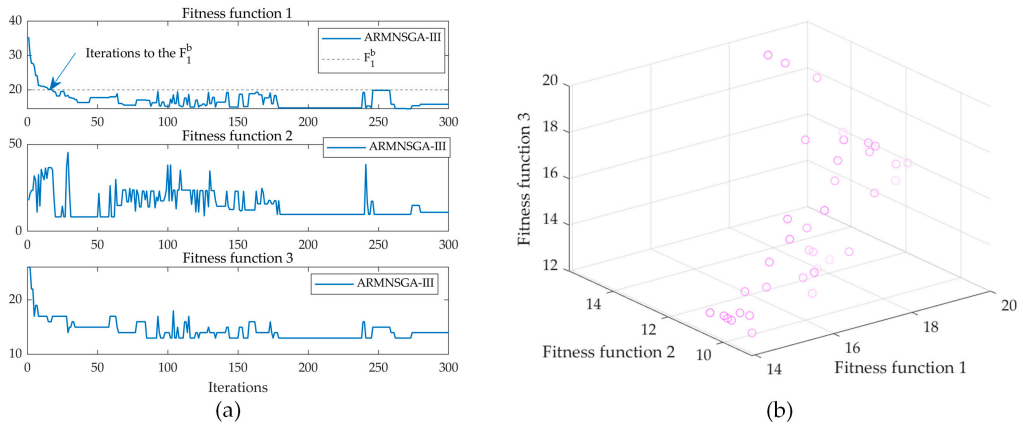


Figure 10. Iterations of the fitness functions and the potential Pareto front. (**a**) shows the variation of fitness functions during the algorithm iterations, (**b**) presents the top-performing individuals as pink dots, the points with darker colors indicate better ASF.

Now we choose one of the best solutions to show the UAV flight path and the performance. In Figure 11, (a) is the optimized flight path with users' weights. The black polyline is the flight path; every UAV takes off and lands in the airport which is the green triangle in the figure, so every polyline forms a closure polygon; the light blue number in flight path marks the serial number of flight path. Meanwhile, (b) presents the flight path with average GDOP in epochs of every grid, where the grids with 0 weights are not calculated. Finally, (c) and Table 2 present decision variables of the optimal results.

Table 2. The optimization results of UAV flight path azimuth (degrees).

Flight Path Serial Number	The number of segments along UAV's flight									
	1	2	3	4	5	6	7	8	9	10
1	96	150	96	102	99	262	282	287	314	296
2	96	100	67	96	96	276	276	247	280	276
3	145	119	149	117	144	324	302	329	327	292
4	95	81	94	73	101	269	253	274	272	275
5	99	94	69	92	101	281	272	249	274	279
6	80	95	82	82	79	259	263	262	265	270
7	142	147	159	159	68	246	323	339	346	319
8	157	151	156	159	157	337	339	336	331	337

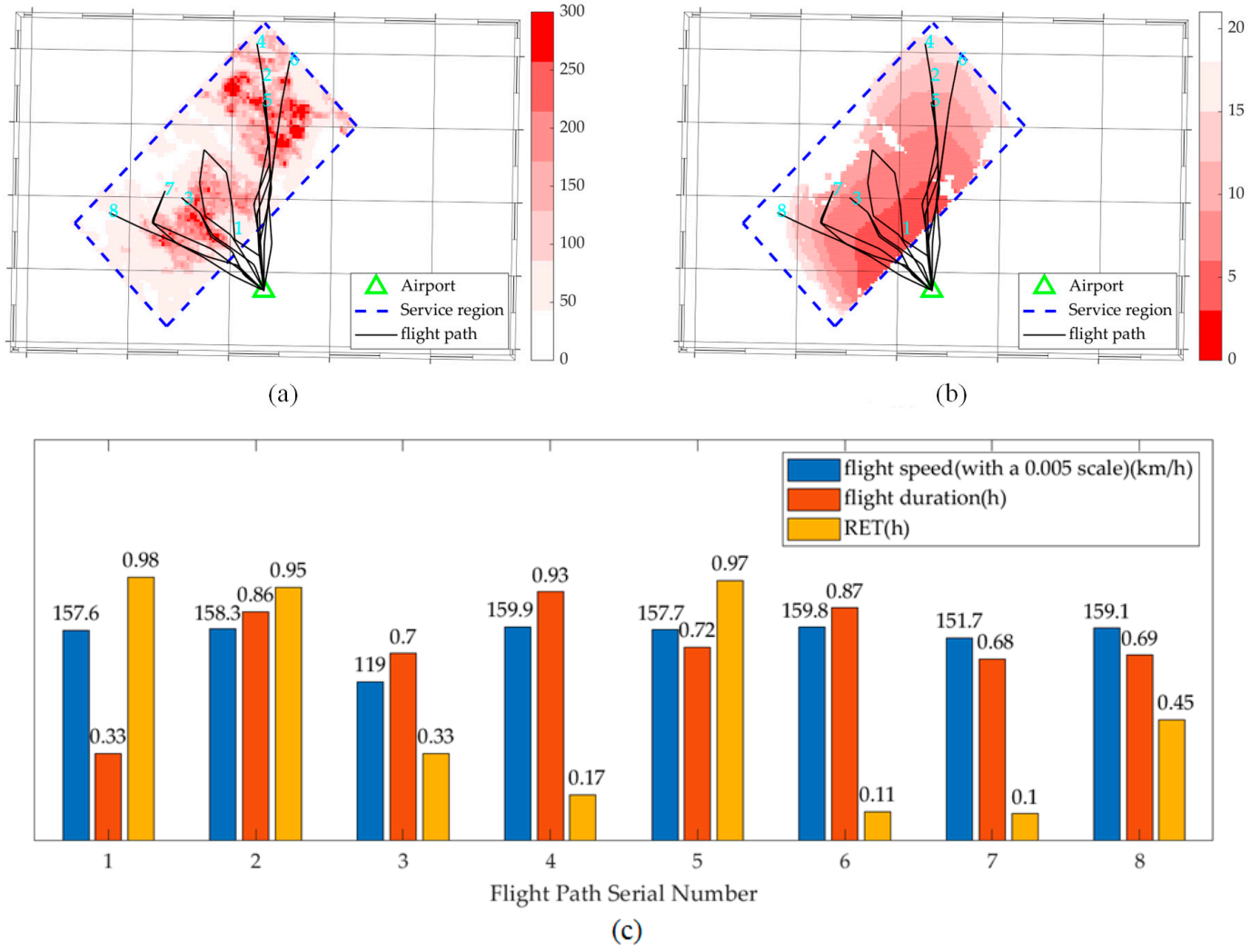


Figure 11. Simulation results of UAV flight path optimization: (**a**) presents the flight path with user distribution and weights, (**b**) presents the flight path with average GDOP in epochs of every grid, and (**c**) presents the decision variables (flight path azimuth in Table 3) in (**a**,**b**).

The algorithm's optimal results indicate the proposed flight paths converge towards regions of higher weights, with many flight paths ultimately exhibiting a simple polyline segment, like 3, 6, and 8. In fact, the UAVs on these flight paths approximately return along the same path. As derived of the theoretical maximum endurance $E^{r,\max}$ in Section 3.1, this kind of flight path can effectively enhance the utilization rate of UAVs. Some flight paths exhibited an approximate spindle shape, like 1, 5, and 7. This type of flight path

effectively utilizes the limited flight duration of the UAV, thus enabling a rapid deployment to the service region and facilitating UAVs' dispersion distribution. According to the principles of SPP, a tetrahedral layout of the positioning base stations relative to users typically yields favorable GDOP metrics. Consequently, the flight paths illustrated in the figure are appropriately dispersed within the service region.

As the system performance, the average E_e in epochs $\overline{E_e} = 9.711$ means that when the user's equivalent ranging error (UERE) is approximately 1 m [17], the user's average positioning accuracy reaches the 10 m level. $F_2 = 22.04$ means there are 22 UAVs performing tasks at any given moment on average; $F_3 = 0.14h$ means it takes 8.4 min to ensure the average number of observable UAVs for the users reaches four visible UAVs. The results indicate the UAV-PNS possesses a basic navigation performance.

To analyze the distribution of the average GDOP in epochs in Figure 10b specifically, the service area was statistically assessed using grid points as units. The variations over time at different grid points will be discussed in detail in the next section. Statistical analysis reveals that on average over the simulation period, 99.98% of users had an average visibility of more than four UAVs. This suggests the feasibility of instantaneous SPP. Regarding user's average GDOP during the simulation period, 98.59% of users had an average GDOP below 20. The position service can be fairly used [34]; as nearly half of users possess an average GDOP below 8, it is a relatively good performance. Subject to the UAV costs, the percentage of users with an average GDOP below 6 is still small. A comparative summary of the statistical results is presented in Table 4.

Table 3. UAV-PNS performance.

UAV-PNS Performance	Value
The first fitness function (F_1)	15.671
Average E_e and S_e in epochs ($\overline{E_e}$ and $\overline{S_e}$)	9.711, 5.96
The second fitness function (F_2)	22.04
The third fitness function (F_3)	0.14 h

In summary, the flight path optimization results provided by the algorithm satisfied the navigation demands of the majority of users in the region, with visible UAV counts exceeding four and moderate position accuracy. However, due to constraints such as the limited UAV count, flight speed, and endurance, a small number of users experience insufficient positioning performance. In practical applications of UAV swarm flight path optimization and system construction, scenarios involving multiple airports for UAV swarm cooperative positioning will be considered. As the diversity and specificity of airport numbers and UAV quantities, the UAV-PNS performance indicated by the algorithm will be significantly improved.

Table 4. Statistical results of users' average positioning performance in epochs.

Metrics	Percentage
Average visible UAV number reach 4	99.98%
Average GDOP < 20	98.59%
Average GDOP < 8	41.24%
Average GDOP < 6	15.17%

4.2.2. Evaluation of Dynamic Performance

To analyze the variation in system performance during the simulation period, typical epochs are selected to reveal the dynamic evolution of UAV-PNS and user GDOP metrics. Figure 12a–d represent the distributions of user instantaneous GDOP and UAV instantaneous positions (represented as light purple circles) on the flight path at 0.15 h, 0.2 h, 0.3 h, and 0.5 h, respectively.

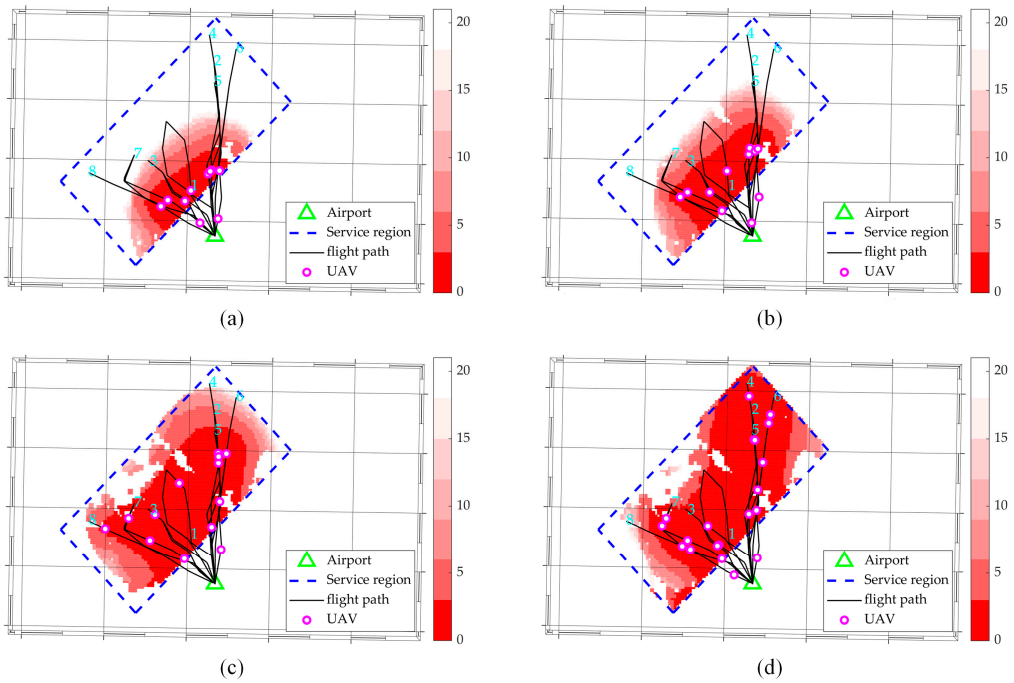


Figure 12. User's instantaneous GDOP in different time after system request: (**a**) presents 0.15 h, (**b**) presents 0.2 h, (**c**) presents 0.3 h, and (**d**) presents 0.5 h.

As for Figure 12a,b, it can be inferred that UAVs dart at the region in the early stage of the flight duration. The system is capable of achieving rapid establishment from external airports to distant regions, effectively utilizing the maneuverability advantages of fixed-wing UAV platforms. Simulation results show the establishment time T_{SE} reaches 0.14 h. Figure 12c,d show the UAV swarm gradually covered the entire region, with users' instantaneous GDOP reaching below 3. This indicates high positioning accuracy while the first batch of UAVs just began to return. It portends users' GDOP metrics became excellent and robust after the UAV-PNS maturely operated.

During the dynamic establishment, the performance of ground grid points was evaluated. We analyzed it in spatial and temporal dimensions: In spatial, the mean GDOP of the best 20%, bottom 20%, and middle 60% of grid users were shown in epochs, respectively, in Figure 13a. In temporal, the percentage changes in grids corresponding to different levels of GDOP were statistically analyzed in epochs, as illustrated in Figure 13b.

According to Figure 13, as the UAVs rapidly approach the service region, there is a significant improvement in the performance of grid points with initially poor positioning metrics. For instance, the red curve in (a) and the yellow curve in (b) exhibit the most pronounced changes across the subplots. The tendency of GDOP is consistent with the establishment time T_{SE} for 0.14 h at the gray dashed vertical line, and remains unstable approximately until 0.4 h. At this point, the curves reach a fluctuation, suggesting that the system has reached a mature state, thus demonstrating that the UAV-PNS architecture proposed in this paper ensures navigation accuracy and robustness for users.

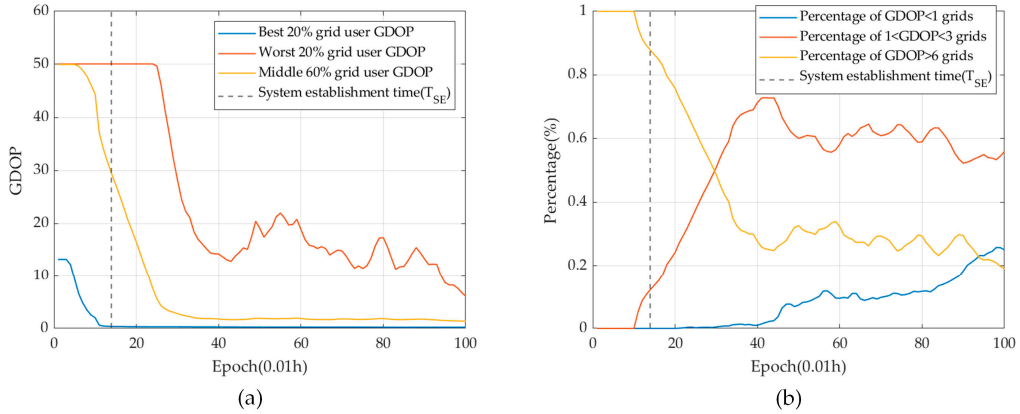


Figure 13. Analysis for grids GDOP in spatial and temporal dimensions during system establishment. (**a**) presents the mean GDOP of the best 20%, bottom 20%, and middle 60% of grid users were shown in epochs, (**b**) presents the percentage changes in grids corresponding to different levels of GDOP.

4.2.3. Performance Analysis of the ARMNSGA-III

This subsection compares the proposed ARMNSGA-III with the NSGA-III method under the same constraints and fitness functions. To analyze the algorithm's efficiency, the same number of iterations is set, allowing for a comparison of the convergence speed.

With the assistance of flight path azimuth and the flight speed acceptance–rejection mutation module, the ARMNSGA-III algorithm reduces the dimensionality of the search space, significantly enhancing search efficiency compared to the NSGA-III. The tendency of the fitness functions for comparing ARMNSGA-III and NSGA-III is illustrated in Figure 14a. Under the same parameter configuration described in Table 1, the fitness function tends to converge around the 50th iterations, indicating that the Pareto front has been approached. It is evident from fitness function 1 that ARMNSGA-III is faster than the NSGA-III to reach the F_1^b, and in the following iterations, ARMNSGA-III achieves better fitness values than the NSGA-III. As for the F_2 and F_3, these fitness functions are of secondary priority. For the F_2, ARMNSGA-III is far better than NSGA-III, while the F_3 is comparable.

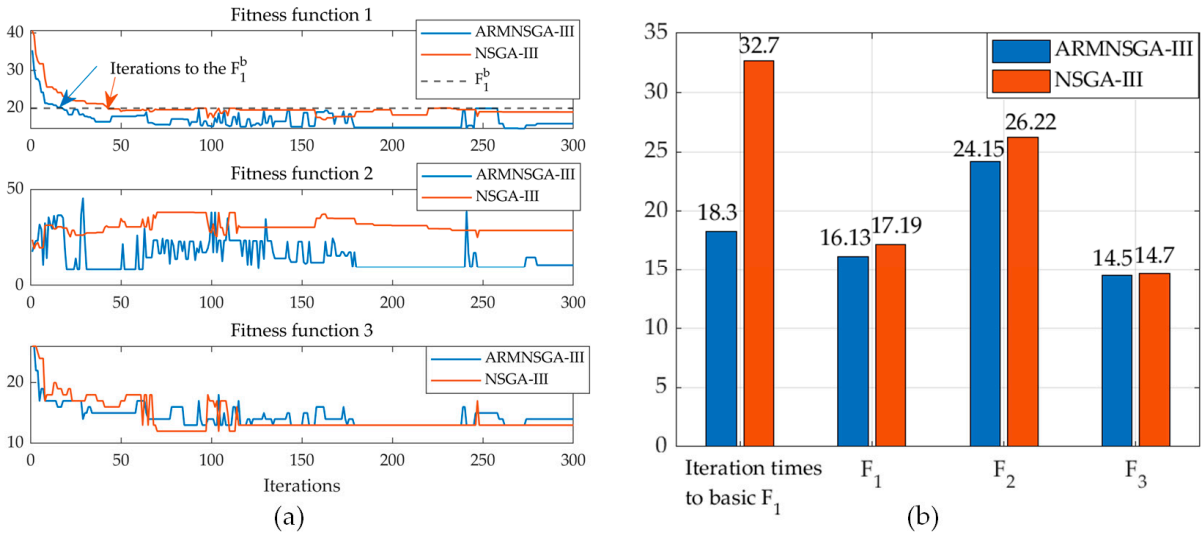


Figure 14. Timeliness efficiency comparison of the ARMNSGA-III and the benchmark method (NSGA-III): (**a**) presents fitness function value convergence during iteration, and (**b**) presents the performance comparison of ARMNSGA-III and NSGA-III results after 100th iteration.

To facilitate performance comparisons, especially in algorithm timeliness, 20 identical simulations were conducted using both the ARMNSGA-III and NSGA-III. As shown in Figure 14b, the tendency of the fitness function from the initial to the 100th iteration was recorded, and the average fitness function results in 20 identical simulations were calculated for comparison.

Figure 14 illustrates that the fitness functions have better results with the use of the ARMNSGA-III; the iterations to F_1^b and the fitness functions (F_1, F_2, F_3) have decreased. The proposed method efficiently extracts and utilizes prior users' weights distribution information, and the mutation strategy enables the population to reach solution space with better fitness values, significantly increasing the likelihood of finding optimal solutions, approaching the Pareto front of the problem. This enhances the timeliness and efficiency of the algorithm, demonstrating stronger optimization capabilities for problems with effective search spaces.

The iteration times to F_1^b, utilizing the optimized search strategy, achieved a 44.01% improvement in our method compared to the NSGA-III in Figure 14b, demonstrating the algorithm's timeliness. Additionally, the fitness functions (F_1, F_2, F_3) decreased by 6.17%, 7.89%, and 1.36% in the 100th iteration, respectively, confirming the ARMNSGA-III effectively enhanced timeliness and search efficiency.

The simulations were conducted using Matlab R2024a(version number: 24.1.0.2537033) on a personal computer with an AMD Ryzen 7 5800H CPU and 32GB of memory, manufactured by lenovo, China.

5. Conclusions

This paper addresses the UAV swarm flight path optimization problem in the UAV-PNS, designing an architecture for PNS based on fixed-wing UAV platforms. Constraints with the flight costs of UAV swarms, an ARMNSGA-III is proposed with multi-objectives. Simulations that validated the rationality of the architectural design, and evaluated the algorithm, are conducted in the scenarios, with results indicating the following:

1. The UAV flight path optimization effectively enhances the service efficiency of the UAV-PNS. Under the constraints of limited costs, a regional UAV-PNS has been constructed, achieving an average visibility of more than four UAVs for 99.98% of users, with good GDOP metrics revealing moderate position accuracy.
2. Dynamic analysis and evaluation of the system's operational process demonstrate that the system fully leverages the maneuverability advantages of UAVs, with an establishment time of 0.14 h, enabling a rapid deployment. After system mature deployment, the instantaneous weighted average and weighted standard deviation of GDOP metrics for users within the region are favorable, ensuring spatial and temporal continuity and uniformity in the system's positioning performance.
3. The ARMNSGA-III proposed in this paper incorporates users' weights distribution and flight path characteristics in its population mutation strategy, and exhibits better timeliness compared to the NSGA-III, achieving a 44.01% improvement, demonstrating superior efficiency.

Future works will focus on the real-time optimization of flight paths and maintaining spatiotemporal reference for INS-assist UAVs, with direct optimization targets related to regional user pseudorange and Doppler positioning accuracy.

Author Contributions: Conceptualization, R.G., H.Y. and Y.Z.; methodology, R.G. and H.Y.; software, R.G.; validation, R.G.; formal analysis, R.G., H.Y. and Y.Z.; investigation, R.G., H.Y., Y.Z., X.C. and G.Z.; resources, H.Y., Y.Z. and X.C.; data curation, R.G.; writing—original draft preparation, R.G.; writing—review and editing, H.Y. and Y.Z.; visualization, R.G.; supervision, H.Y. and Y.Z.; project

administration, H.Y., Y.Z. and X.C.; funding acquisition, Y.Z. All authors have read and agreed to the published version of the manuscript.

Funding: This research was funded by the Key Laboratory Fund Project for Simulation of Complex Electronic Systems (614201004022210), the Chinese Academy of Sciences Youth Innovation Promotion Association (2022126), the National Key Research and Development Plan (2022YFC2204700), the Beijing Natural Science Foundation (1234041).

Data Availability Statement: The data presented in this study are openly available in https://human-settlement.emergency.copernicus.eu/ghs_pop2023.php at 10.2905/2FF68A52-5B5B-4A22-8F40-C41DA8332CFE (accessed on 1 February 2025).

Conflicts of Interest: The authors declare no conflicts of interest.

References

1. Morton, Y.J.; van Diggelen, F.; Spilker, J.J., Jr.; Parkinson, B.W.; Lo, S.; Gao, G. *Position, Navigation, and Timing Technologies in the 21st Century*; Wiley: Hoboken, NJ, USA, 2021; Volume 1, ISBN 978-1-119-45841-8.
2. Li, X.; Zhang, P.; Huang, G.; Zhang, Q.; Guo, J.; Zhao, Y.; Zhao, Q. Performance analysis of indoor pseudolite positioning based on the unscented Kalman filter. *GPS Solut.* **2019**, *23*, 79. [CrossRef]
3. Laoudias, C.; Moreira, A.; Kim, S.; Lee, S.; Wirola, L.; Fischione, C. A survey of enabling technologies for network localization, tracking, and navigation. *IEEE Commun. Surv. Tutor.* **2018**, *20*, 3607–3644. [CrossRef]
4. Barnes, J.; Rizos, C.; Kanli, M.; Pahwa, A. A positioning technology for classically difficult GNSS environments from Locata. In Proceedings of the IEEE/ION PLANS 2006, San Diego, CA, USA, 25–27 April 2006; pp. 715–721.
5. Barnes, J.; Rizos, C.; Wang, J.; Small, D.; Voigt, G.; Gambale, N. High precision indoor and outdoor positioning using LocataNet. *J. Glob. Position. Syst.* **2003**, *2*, 73–82. [CrossRef]
6. LeMaster, E.A.; Rock, S.M. A local-area GPS pseudolite-based navigation system for mars rovers. *Auton. Robot.* **2003**, *14*, 209–224. [CrossRef]
7. Crommelinck, S.; Bennett, R.; Gerke, M.; Yang, M.Y.; Vosselman, G. Contour detection for UAV-Based cadastral mapping. *Remote Sens.* **2017**, *9*, 171. [CrossRef]
8. Xiang, L.; Zhang, M.; Klein, A. Robust Dynamic Trajectory Optimization for UAV-Aided Localization of Ground Target. In Proceedings of the GLOBECOM 2023—2023 IEEE Global Communications Conference, Kuala Lumpur, Malaysia, 4–8 December 2023; pp. 7484–7489.
9. Amt, J.H.; Raquet, J.F. Flight testing of a pseudolite navigation system on a UAV. In Proceedings of the 2007 National Technical Meeting of the Institute of Navigation, San Diego, CA, USA, 22–24 January 2007; pp. 1147–1154.
10. Tuohino, J.L.; Farley, M.G.; James, R.R. Military pseudolite flight test results. In Proceedings of the 13th International Technical Meeting of the Satellite Division of the Institute of Navigation (ION GPS 2000), Salt Lake City, UT, USA, 19–22 September 2000; pp. 2079–2088.
11. Kim, E. A coverage analysis methodology for APNT pseudolite ground network. In Proceedings of the 24th International Technical Meeting of the Satellite Division of the Institute of Navigation (ION GNSS 2011), Portland, OR, USA, 20–23 September 2011; pp. 495–507.
12. Yin, L.; Ni, Q.; Deng, Z. A GNSS/5G integrated positioning methodology in D2D communication networks. *IEEE J. Sel. Areas Commun.* **2018**, *36*, 351–362. [CrossRef]
13. Dou, Z.; Yao, Z.; Lu, M. Distributed radio local positioning system spatial reference autonomous establishment technology. *Acta. Electron. Sin.* **2022**, *50*, 841–848.
14. Wu, Z.; Yao, Z.; Lu, M. Waypoint selection for unmanned aerial vehicle-aided calibration in wireless positioning networks. *IET Radar Sonar Navig.* **2023**, *17*, 1088–1099. [CrossRef]
15. Yang, X.; Liu, W.; Ye, X.; Li, X.; Wei, S.; Wang, F. A geometry-based method for the rapid deployment of a UAV pseudolite navigation system in a target area. *J. Geod.* **2023**, *97*, 90. [CrossRef]
16. Qu, Y.; Wang, S.; Zeng, L.; Gong, Y. Path planning algorithm for airborne pseudolites installed on stratospheric airships. *J. Beijing Univ. Aeronaut. Astronaut.* **2021**, *49*, 1071–1082.
17. Teng, Y.; Wang, J. A closed-form formula to calculate geometric dilution of precision (GDOP) for multi-GNSS constellations. *GPS Solut.* **2016**, *20*, 331–339. [CrossRef]
18. Gugan, G.; Haque, A. Path planning for autonomous drones: Challenges and future directions. *Drones* **2023**, *7*, 169. [CrossRef]
19. Tan, C.; Xu, Y.; Luo, R.; Li, Y.; Yuan, C. Low Earth orbit constellation design using a multi-objective genetic algorithm for GNSS reflectometry missions. *Adv. Space Res.* **2023**, *71*, 2357–2369. [CrossRef]

20. Ge, H.; Li, B.; Nie, L.; Ge, M.; Schuh, H. LEO constellation optimization for LEO enhanced global navigation satellite system (LeGNSS). *Adv. Space Res.* **2020**, *66*, 520–532. [CrossRef]
21. Zhang, Y.; Li, Z.; Wang, Z.; Li, R.; Yuan, H. The improvement of BDS Observation Geometry with LEO constellations in Orbit Determination. *Measurement* **2021**, *177*, 109228. [CrossRef]
22. Zhang, Y.; Li, Z.; Li, R.; Wang, Z.; Yuan, H.; Song, J. Orbital design of LEO navigation constellations and assessment of their augmentation to BDS. *Adv. Space Res.* **2020**, *66*, 1911–1923. [CrossRef]
23. Guan, M.; Xu, T.; Gao, F.; Nie, W.; Yang, H. Optimal walker constellation design of LEO-based global navigation and augmentation system. *Remote Sens.* **2020**, *12*, 1845. [CrossRef]
24. Ma, F.; Zhang, X.; Li, X.; Cheng, J.; Guo, F.; Hu, J.; Pan, L. Hybrid constellation design using a genetic algorithm for a LEO-based navigation augmentation system. *GPS Solut.* **2020**, *24*, 62. [CrossRef]
25. Xue, W.; Hu, M.; Ruan, Y.; Wang, X.; Yu, M. Research on Design and Staged Deployment of LEO Navigation Constellation for MEO Navigation Satellite Failure. *Remote Sens.* **2024**, *16*, 3667. [CrossRef]
26. Huang, R.; Zhao, L.; Chen, Z. A Technique of Pseudolite Cooperative Layout Based on Particle Swarm Optimization Algorithm in GNSS Ground Based Augmentation Systems. In Proceedings of the 2021 IEEE 2nd International Conference on Information Technology, Big Data and Artificial Intelligence (ICIBA), Chongqing, China, 17–19 December 2021; Volume 2, pp. 1064–1068.
27. Huang, J.; Tao, Z.; He, J. Deep Reinforcement Learning Method of UAV Behavior Planning for Optimizing Geometric Dilution Precision Distribution. In Proceedings of the 2022 5th International Conference on Advanced Electronic Materials, Computers and Software Engineering (AEMCSE), Wuhan, China, 22–24 April 2022; pp. 276–280.
28. Ho, L.; Jangsher, S. UAV Trajectory Optimization based on Predicted User Locations. In Proceedings of the 2024 IEEE Wireless Communications and Networking Conference (WCNC), Dubai, United Arab Emirates, 21–24 April 2024; pp. 1–6.
29. Meng, X.; Roberts, G.; Dodson, A.; Cosser, E.; Barnes, J.; Rizos, C. Impact of GPS satellite and pseudolite geometry on structural deformation monitoring: Analytical and empirical studies. *J. Geod.* **2004**, *77*, 809–822. [CrossRef]
30. Han, G.; Yang, X.; Liu, L.; Zhang, W.; Guizani, M. A disaster management-oriented path planning for mobile anchor node-based localization in wireless sensor networks. *IEEE Trans. Emerg. Top. Comput.* **2017**, *8*, 115–125. [CrossRef]
31. Leune, T.; Wehs, T.; Janssen, M.; Koch, C.; von Cölln, G. Optimization of wireless locating in complex environments by placement of anchor nodes with evolutionary algorithms. In Proceedings of the 2013 IEEE 18th Conference on Emerging Technologies & Factory Automation (ETFA), Cagliari, Italy, 10–13 September 2013; pp. 1–6.
32. Raymer, D. *Aircraft Design: A Conceptual Approach*; American Institute of Aeronautics and Astronautics, Inc.: Washington, DC, USA, 2012.
33. Zhang, X.; Chen, J.; Xin, B.; Peng, Z. A memetic algorithm for path planning of curvature-constrained UAVs performing surveillance of multiple ground targets. *Chin. J. Aeronaut.* **2014**, *27*, 622–633. [CrossRef]
34. Tahsin, M.; Sultana, S.; Reza, T.; Hossam-E-Haider, M. Analysis of DOP and its preciseness in GNSS position estimation. In Proceedings of the 2015 International Conference on Electrical Engineering and Information Communication Technology (ICEEICT), Savar, Dhaka, Bangladesh, 21–23 May 2015; pp. 1–6.
35. Lappas, I.; Bozoudis, M. The development of an ordinary least squares parametric model to estimate the cost per flying hour of 'Unknown' aircraft types and a comparative application. *Aerospace* **2018**, *5*, 104. [CrossRef]
36. Deb, K.; Jain, H. An evolutionary many-objective optimization algorithm using reference-point-based nondominated sorting approach, part I: Solving problems with box constraints. *IEEE Trans. Evol. Comput.* **2013**, *18*, 577–601. [CrossRef]
37. Tian, Y.; Si, L.; Zhang, X.; Cheng, R.; He, C.; Tan, K.C.; Jin, Y. Evolutionary large-scale multi-objective optimization: A survey. *ACM Comput. Surv. CSUR* **2021**, *54*, 1–34. [CrossRef]
38. Tian, Y.; Cheng, R.; Zhang, X.; Jin, Y. PlatEMO: A MATLAB platform for evolutionary multi-objective optimization [educational forum]. *IEEE Comput. Intell. Mag.* **2017**, *12*, 73–87. [CrossRef]
39. Neumann, V. Various techniques used in connection with random digits. *Notes GE Forsythe* **1951**, *3*, 36–38.
40. Wang, X.; Meng, Q. Continuous-time dynamic network yield management with demand driven dispatch in the airline industry. *Transp. Res. Part E Logist. Transp. Rev.* **2008**, *44*, 1052–1073. [CrossRef]
41. Locatelli, M.; Schoen, F. Random Linkage: A family of acceptance/rejection algorithms for global optimisation. *Math. Program.* **1999**, *85*, 379–396. [CrossRef]
42. Schiavina, M.; Freire, S.; MacManus, K. *GHS-POP R2023A-GHS Population Grid Multitemporal (1975–2030)*; Joint Research Centre Data Catalogue, the European Commission: Brussels, Beligum, 2022.

Disclaimer/Publisher's Note: The statements, opinions and data contained in all publications are solely those of the individual author(s) and contributor(s) and not of MDPI and/or the editor(s). MDPI and/or the editor(s) disclaim responsibility for any injury to people or property resulting from any ideas, methods, instructions or products referred to in the content.